AGU PUBLICATIONS

Geophysical Research Letters

RESEARCH LETTER
10.1002/2016GL070622

Key Points:
- Tropopause-level cooling occurs in tropical cyclones starting several days prior to maximum intensity
- Tropopause-level cooling has a similar magnitude as the warm core
- Tropopause-level cooling may affect tropical cyclone potential intensity

Correspondence to:
L. Rivoire,
lrivoire@colostate.edu

Citation:
Rivoire, L., T. Birner, and J. Knaff (2016), Evolution of the upper-level thermal structure in tropical cyclones, *Geophys. Res. Lett.*, *43*, 10,530–10,537, doi:10.1002/2016GL070622.

Received 6 APR 2016
Accepted 19 SEP 2016
Accepted article online 24 SEP 2016
Published online 15 OCT 2016

Evolution of the upper-level thermal structure in tropical cyclones

Louis Rivoire[1], Thomas Birner[1], and John A. Knaff[2]

[1]Department of Atmospheric Science, Colorado State University, Fort Collins, Colorado, USA, [2]NOAA Center for Satellite Applications and Research, Fort Collins, CO, USA

Abstract Tropical cyclones (TCs) are associated with tropopause-level cooling above tropospheric warming. We collect temperature retrievals from 2007 to 2014 near worldwide hurricane-strength TCs using three remote sensing platforms: the Constellation Observing System for Meteorology, Ionosphere, and Climate (COSMIC), the Advanced Microwave Sounding Unit-A (AMSU-A), and geostationary infrared (IR) imagery. These retrievals are composited about the lifetime maximum intensity (LMI) to examine the evolution of the fine-scale temperature structure within TCs. The convective structure evolves highly asymmetrically about LMI, while intensity evolution shows a much weaker degree of asymmetry. Relative to the far-field structure, tropopause-level cooling occurs before a tropospheric warm core is established. We speculate that the associated convective destabilization exerts a positive feedback on TC development by increasing the depth of existing convection. Tropopause-level cold anomalies move away from the storm after LMI, potentially increasing the near-surface horizontal pressure gradient toward the storm center and increasing the maximum winds.

1. Introduction

Tropical cyclones are characterized by a low-pressure cyclonic vortex at the center of a region of mesoscale convection. The middle to upper troposphere (UT) exhibits a warm core, which is a well-known feature and is understood as a direct response to the release of latent heat acquired from the ocean through deep convection [*Emanuel*, 1991]. The response in the upper troposphere/lower stratosphere (UTLS) has been documented by early studies, although its evolution during the lifetime of TCs is less explored. *Arakawa* [1951] illustrated "the upward displacements and cold air in the field of annular tropopause ridge in the storm area," and *Koteswaram* [1967] described an "upper cold core." The generic response to tropical deep convection (not necessarily associated with TCs) was described as a "significant cold anomaly atop the mesoscale anvils" by *Johnson and Kriete* [1982], and more recently, *Holloway and Neelin* [2007] termed it the "convective cold top." Observational studies, e.g., *Paulik and Birner* [2012] and *Biondi et al.* [2013], found the coldest anomalies above 15 km and near the tropopause with an amplitude of several kelvins.

Holloway and Neelin [2007] have attributed the tropopause-level cooling to hydrostatic pressure gradients extending above the diabatic heating source, triggering divergence, ascent, and adiabatic cooling aloft. This is consistent with the effects of the forced secondary circulation ("in-up-out" [*Möller and Montgomery*, 2000]) that accompanies eyewall diabatic heating [*Pendergrass and Willoughby*, 2009] and causes ascent and divergence aloft and outside the eyewall.

Emanuel and Rotunno [2011] have pointed out that the outflow temperature and thus the outflow entropy are set, at least in part, by the internal storm dynamics (referred to by these authors as outflow self-stratification, which they hypothesize is "set in the storm's core by the requirement that the Richardson number remain near its critical value for the onset of small-scale turbulence"). *Molinari et al.* [2014] suggested further that cloud-radiative cooling also contributes to low Richardson number in the outflow layer. Regardless of the precise mechanisms involved, the idea that the outflow temperature is set by the storm itself suggests an important feedback between outflow structure and storm intensity.

If the relatively large tropospheric heating and balanced circulation of TCs produce the cooling response near the tropopause, the cooling itself might exert a feedback by destabilizing the upper levels, potentially deepening existing convection. In light of these mechanisms, this study intends to provide an improved description of the evolution of the thermal structure in TCs in the UTLS region. High vertical resolution GPS radio occultation

(GPS-RO) measurements from the Constellation Observing System for Meteorology, Ionosphere, and Climate (COSMIC), and high horizontal resolution measurements from the Advanced Microwave Sounding Unit-A (AMSU-A) on board operational satellites are combined to provide an unprecedented view of TCs worldwide. Infrared (IR) imagery from geostationary satellites allows us to observe fine-scale thermal structures in the horizontal direction and to analyze the distribution of convection in TC systems.

2. Data and Methods

2.1. COSMIC Temperature

Radio occultation uses Doppler shifts in GPS radio signals detected by low-orbiting satellites to retrieve bending angle profiles in the atmosphere. Bending angle is primarily related to the temperature, pressure, and water vapor content of the atmosphere. The COSMIC Data Analysis and Archival Center (CDAAC) processes bending angle data to provide temperature profiles with high accuracy, precision, and vertical resolution, especially between 5 and 25 km height [*Kuo et al.*, 2004]. COSMIC profiles are available for all weather conditions and have a global distribution that peaks in the subtropics and midlatitudes (e.g., *Son et al.* [2011]). In the UTLS, these measurements are the only source of space-based data unaffected by clouds. *Biondi et al.* [2012] demonstrated that GPS-RO data can be used to detect vertical thermal structures in strong convective systems. The contribution of the water content to the bending angle is considered negligible for temperatures less than 250 K [*Kursinski et al.*, 1996], directly allowing retrieval of the temperature and pressure at upper levels (these profiles are referred to as "dry retrievals"). In the lower troposphere where the water content affects the bending angle, temperature estimates from 1-D variational analysis using the European Centre for Medium-Range Weather Forecasting (ECMWF) low-resolution analysis data are used to retrieve profiles of temperature, pressure, and water vapor (referred to as "wet retrievals"). However, such estimates can be of poor quality in regions of large horizontal gradients [*Davis and Birner*, 2016]. TCs can be expected to be misrepresented in meteorological analyses and are therefore likely to be misrepresented in the wet retrievals. This study therefore focuses on the UTLS region where temperature profiles are most accurate. Wet retrievals will be used as a qualitative complement to dry retrievals below 10 km.

COSMIC profiles are collected near 6 hourly TC best track locations from the Automated Tropical Cyclone Forecast (ATCF) [*Sampson and Schrader*, 2000] system archive (ATCF data are from the National Hurricane Center and the Joint Typhoon Warning Center). These profiles are then positioned about the time of first lifetime maximum intensity (LMI) determined using intensities from the ATCF database. Intensities are based on 1 min sustained wind speeds. Intensities equal to the LMI can be reached several times during the lifetime of one TC; here LMI will refer only to the first such maximum for each TC. Individual temperature profiles are linearly interpolated onto a regular 200 m vertical grid, corresponding to the typical vertical resolution of GPS-RO data near the tropopause [*Kursinski et al.*, 2001]. Profiles are assigned to the nearest neighboring best track point (in space), allowing a maximum time offset of 5 h. This time, offset was chosen after careful consideration in order to improve statistics, and each COSMIC profile is used only once. Profiles are collected up to 1500 km away from the storm center, although it should be noted that the convective region in TCs has a typical radius of 400–700 km [*Frank*, 1977]. Data collected outside TC systems provides background information and gives insights into the horizontal extent of temperature anomalies associated with TCs. This sampling process is repeated for the hurricane-strength TCs (LMI $\geq$ 64 kt or 33 m s^{-1}) occurring within $\pm$35° of latitude in 2007–2014, allowing the collection of over 33,000 radio occultation profiles near 322 storms around the globe. This large amount of data is required to overcome the substantial variability in the vertical structure of TCs and draw robust conclusions [*Stern and Nolan*, 2009]. Note that profiles collected over land are included in the study as we found their impact on our results to be small. Finally, profiles collected poleward of $\pm$35° of latitude are not included to avoid sampling poleward of the subtropical jets.

Composites of temperature anomalies are built based on the time of LMI to reveal the evolution of the thermal structure in TCs. Anomalies are displayed relative to two backgrounds: the monthly climatological background from the COSMIC data set, interpolated to each COSMIC profile (referred to as "local climatology") and the area average between 1300 and 1500 km away from the storm center (referred to as the "far-field background"). Using the local climatology emphasizes temporal anomalies, whereas using the far-field background emphasizes spatial anomalies. Radial composites are also constructed to unveil horizontal structures.

2.2. AMSU-A Temperature

TC microwave temperature analyses are byproducts of an operational procedure that provides intensity and surface wind estimates for TCs as described in *Demuth et al.* [2006]. AMSU-A temperatures, along with real-time

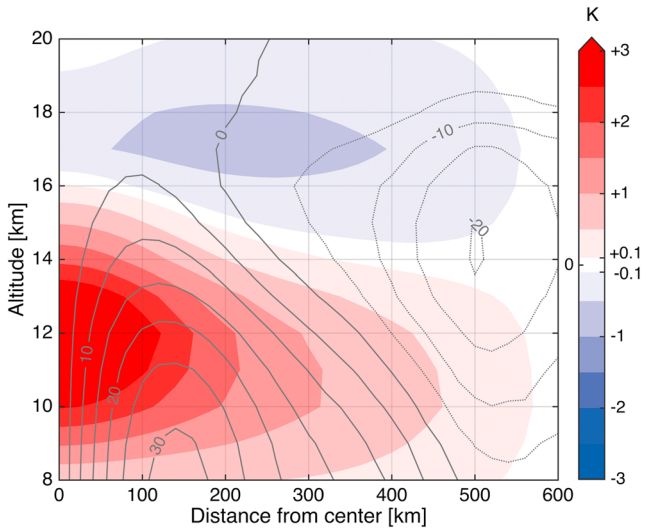

Figure 1. Temperature anomaly from AMSU-A within 3 h of LMI as a function of radius and altitude (above 8 km). Shaded contours show the temperature anomaly, grey contours show the tangential wind in m s^{-1} estimated from the height gradients calculated from AMSU-A temperatures using boundary conditions from the Global Forecast System as in *Demuth et al.* [2004], assuming 1-D gradient balance. Anomalies are relative to the temperature at 600 km. Solid (dotted) wind contours show the cyclonic (anticyclonic) flow.

operational estimates of TC locations, are the primary inputs for this product. The temperature retrieval uses limb corrections for scan position and viewing angle [*Goldberg et al.*, 2001] and a linear retrieval operator derived from collocated rawindsonde data [*Knaff et al.*, 2000] that provides temperature as a function of pressure at 40 levels from 1000 to 0.1 mbar, up to 600 km away from the storm center. Composites of temperature anomalies are constructed based on the time of LMI using the same TC tracks as in section 2.1. Anomalies are relative to the temperature observed at the 600 km radius at each pressure level.

2.3. Infrared Brightness Temperature

Brightness temperature (T_b) provides information about the temperature of cloud tops found in TCs and is a proxy for convective vigor. The analyses of IR T_b used are derived from data collected by the constellation of geostationary satellites. The central wavelength of these data is located in the IR window near 11 μm, where T_b is within a few degrees of the emitting surface conditions in the absence of clouds. The Cooperative Institute for Research in the Atmosphere archives T_b analyses within 600 km of TCs with at least an hourly temporal resolution and a precision of 0.5–1 K. Additional information appears in *Knaff et al.* [2014]. We composite these analyses hourly about the time of LMI using the same TC tracks as in section 2.1.

3. Results Based On High Horizontal Resolution IR and Microwave Data

Figure 1 shows the azimuthally averaged horizontal temperature structure in TCs inferred from AMSU-A data at LMI with a horizontal resolution of ~70 km and a vertical resolution of 1–3 km. The UT warming bulges upward near the storm center where the convective activity is strongest. Tropopause-level cooling occurs at 17 km above sea level (~100 mbar, above the core of the outflow layer) as shown in *Koteswaram* [1967] and peaks at ~200 km away from the storm center, which is well outside the typical radius of the eye (15–30 km [*Weatherford and Gray*, 1988]) and the associated warm subsidence region. The amplitudes of the anomalies (+3.7 K, −0.7 K) are smaller than those found by case studies (+10 to +13 K, −8 to −10 K [e.g., *Koteswaram*, 1967). This may be caused by the large variability in the vertical structure of the TCs that are composited [*Stern and Nolan*, 2009] and by the relatively limited vertical resolution of AMSU compared to the relatively small vertical extent of the tropopause-level cooling (cf. Figure 3).

Figure 2 shows the evolution of the azimuthally averaged T_b in TCs inferred from IR images, and of TC intensity, relative to LMI. IR data show that the coldest cloud tops occur before LMI; in other words, the convective structure evolves asymmetrically about LMI. In comparison, the intensity of TCs evolves with a much weaker degree of asymmetry. Between −4 and −2 days, low T_b is associated with the presence of deep convective outbursts within a few hundred kilometers of the storm center. Between −2 and 0 days, T_b is consistent with

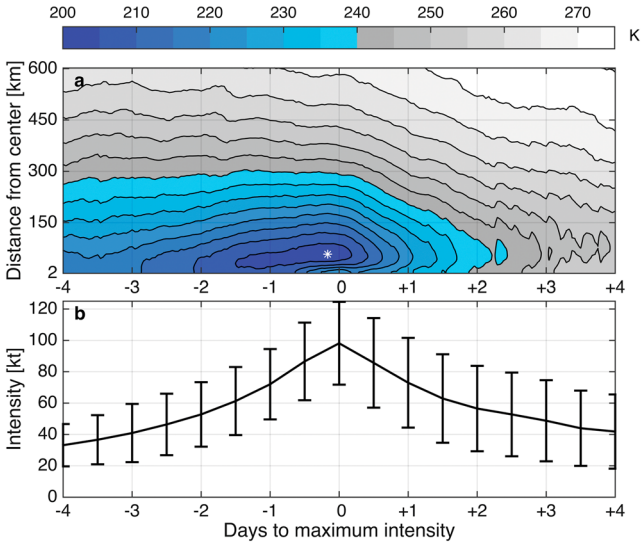

Figure 2. (a) Azimuthally averaged brightness temperature in TCs contoured as a function of time relative to LMI and radius. The temporal resolution is hourly and the radial resolution is 4 km. The white asterisk indicates the minimum value of T_b (202 K). (b) Average intensity of hurricane-strength storms between ±35° of latitude in ATCF, as a function of time relative to LMI. Error bars indicate ±1 standard deviation every 12 h.

the formation of a sustained ring of deep convective clouds between the outer edge of the eye and 100 km away from the storm center [e.g., *Heymsfield et al.*, 2001; *Buontempo et al.*, 2006, 2001]. As TCs move towards latitudes with lower sea surface temperatures, both their intensity and the heights reached by deep convection decrease rapidly, which translates to greater T_b after LMI. Within 30 km of the storm center at LMI, greater T_b offers evidence of eyes with relatively clearer air due to subsidence.

4. Results Based On High Vertical Resolution GPS-RO Data

Temperature anomalies inferred from GPS-RO measurements are shown in Figure 3. Anomalies within 600 km of the storm center (as for AMSU) and 24 h of LMI are shown relative to both the local climatology and far-field background. In the UT, water vapor amounts are small enough that moist and dry adiabats are essentially the same (~9.8 K km^{-1}). The climatological lapse rate is close to 8 K km^{-1} [*Gettelman et al.*, 2011], and the anomalous thermal structure shown in Figure 3 increases this lapse rate by almost 1 K km^{-1}, which is about halfway towards the dry adiabat. The altitude of the largest anomalies is similar to that found in Figure 1 and consistent with *Biondi et al.* [2013]. The tropopause-level cooling is more pronounced here than in Figure 1, likely because GPS-RO has a finer vertical resolution than AMSU. Wet retrievals have a significant warm bias above 15 km (not shown). The difference between the two curves indicates that the far-field UT (above 11 km) is on average warmer than the climatological UT near the storm center.

Figure 4 shows temperature anomalies contoured as a function of distance from the storm center and altitude for 48 h wide temporal bins centered on −2, 0, 2, and 4 days from LMI, with a 200 km radial resolution. Anomalies are defined with respect to the far-field background. At LMI, the horizontal extent of the tropopause-level cooling reaches a peak, while that of the UT warming is still expanding. UT warming bulges upward near the storm center like in Figure 1, although not as noticeably. At +2 days, the UT warming reaches its maximum radial extent while the tropopause-level cooling weakens and clearly dissociates itself from the storm center. At +4 days, a faint tropopause-level cooling is still evident between 400 and 700 km. The UT warming remains as strong as it was at LMI, either indicating stabilization of the storm or a bias due to the undersampling of the inner core region.

Figure 5 compares the evolution of the vertical structure of temperature anomalies in TCs relative to the local, climatological background (top), with anomalies relative to the far-field background (bottom). Relative to the local climatology (Figure 5, top), both the warm and cold signals become stronger and deeper as TCs develop. The warm core weakens beyond +4 days, although fewer data points are included in the composite after that time. The tropopause-level signal thickens after LMI, when TCs are at a latitude of 20° ± 6° on average—where

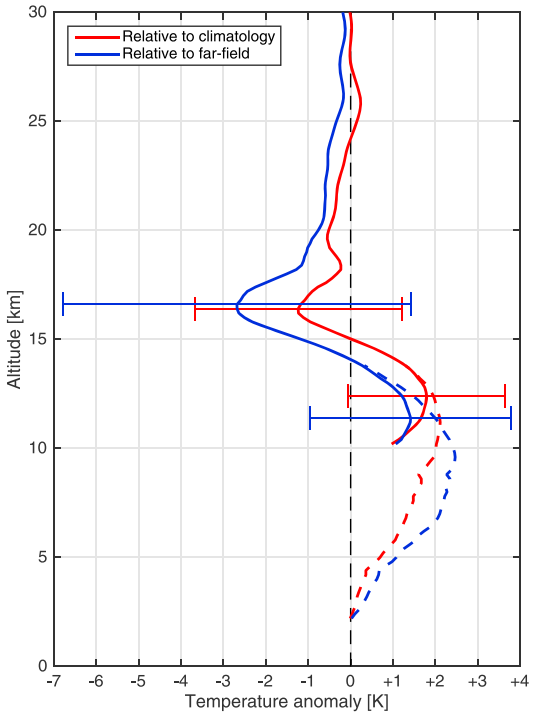

Figure 3. Average temperature anomaly for all COSMIC profiles collected within 600 km and 24 h of LMI. Solid (dashed) lines are the dry (wet) retrievals. Error bars show ±1 standard deviation at the location of the largest anomalies in the dry retrievals.

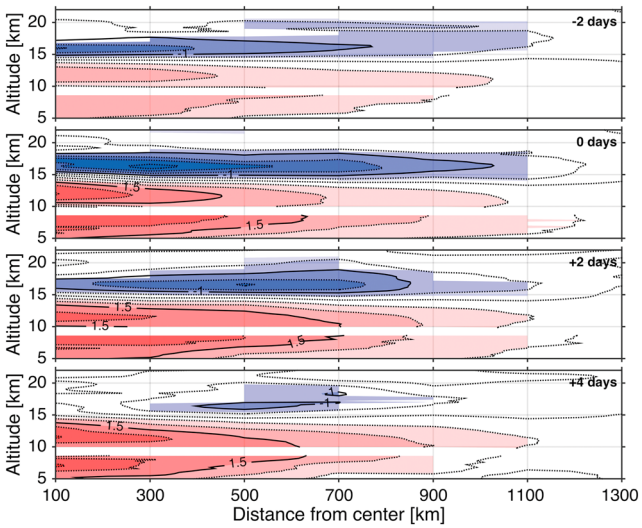

Figure 4. Temperature anomaly from COSMIC contoured for various times before and after LMI as a function of the distance from the center of storms and altitude. Solid contours are at −1 and +1.5 K, dotted contours are every 0.5 K. Anomalies exceeding the *t* test 95% significance level are shaded. Anomalies are relative to the area average between 1300 and 1500 km away from the storm center at each height. The composite includes data from −3 to +5 days, and TC tracks that cover at least the period from −2 days to +4 days are used. The white horizontal band just below 10 km separates dry and wet retrievals. Each panel corresponds to a 48 h wide window, and the radial resolution is 200 km.

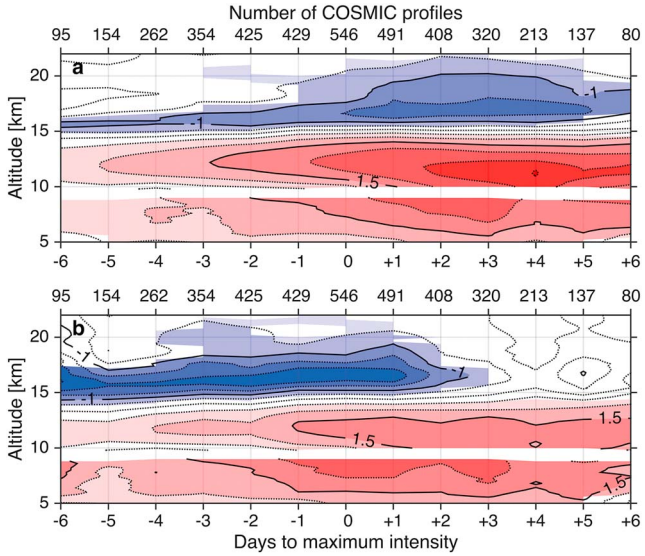

Figure 5. Temperature anomaly from COSMIC within 500 km of TCs contoured as a function of time relative to the time of LMI and altitude. Solid contours are at −1 and +1.5 K, and dotted contours are every 0.5 K. Anomalies exceeding the *t* test 95% significance level are shaded. Anomalies are (a) relative to the local climatology and (b) are relative to the area average between 1300 and 1500 km away from the storm center. Horizontal labels apply to both panels. The white horizontal band just below 10 km separates dry and wet retrievals. The temporal resolution is 1 day.

the climatological tropopause warms when moving poleward [*Seidel et al.*, 2001]. Tropopause-level anomalies extend far outside the 500 km radius (not shown) and indicate large-scale poleward transport of cold, dry air.

The far-field background (Figure 5, bottom) reveals an anomalously cold tropopause several days before LMI, analogous to the development of the coldest cloud tops in Figure 2. The cooling quickly decays after +1 days, in agreement with tropopause-level anomalies moving away from the storm center (Figure 4). This decay coincides with rapidly increasing T_b near the storm center (Figure 2). UT warming persists after LMI, although it should be noted that a few days after LMI, the weaker storms have dissipated and are therefore not included in our sample.

The differences between the top and bottom panels of Figure 5 for the dry retrievals indicate that the far-field UT is warmer than the climatological UT near the storm center (as in Figure 3) during the lifetime of TCs. The far-field UTLS (15–18 km) is warmer than the climatological UTLS at the location of the storm during tropical cyclogenesis. For both backgrounds, the larger the LMI, the larger the amplitude of the anomalous thermal structures (not shown).

5. Discussion and Conclusions

Leveraging the 200 m vertical resolution of GPS-RO, the ~70 km horizontal resolution of AMSU-A data, and the ~4 km horizontal resolution of geostationary IR images, we were able to analyze the composite fine-scale thermal and convective structure in TCs. The composite analyses presented here show the expected qualitative behavior of middle to upper tropospheric warming and tropopause-level cooling. They also reveal that the tropopause-level cooling precedes the warm core signal when measured relative to the far-field structure around storms. This is consistent with the presence of cold cloud tops near the storm center during the intensification period found in IR data, the convective bursts that *Rogers et al.* [2013] found in intensifying TCs, and the lag between the convective intensification and the response of the vortex [*Steranka et al.*, 1986].

Cold anomalies at the tropopause locally destabilize the atmosphere to convection, which may exert a feedback on the depth of the existing convection. Since the cold anomalies precede the establishment of a warm core, the upper-level destabilization might play a role in priming the eyewall updraft that *Willoughby* [1998] described as a "heat pump." This might reinforce the diabatically driven secondary circulation and indirectly stiffen the vortex to vertical wind shear [*Reasor et al.*, 2004], which is of particular importance during the early stages of tropical cyclogenesis.

The dissociation of tropopause-level anomalies from the storm center and their dissipation after LMI indicate radial outward transport near the tropopause (above the core of the outflow layer) and a decrease in the upper-level adiabatic cooling near the storm center, respectively. The latter can be understood as a decrease in the height reached by the eyewall branches of the secondary circulation: idealized experiments by *Schubert and McNoldy* [2010] showed horizontally elongated, vertically compressed secondary circulations for weak vortices and vice versa for strong vortices. Remains of cold air masses lie near the tropopause between 400 and 700 km, essentially inward of the radius of maximum tangential anticyclonic winds in the UTLS [*Frank*, 1977]. Integrating the hydrostatic relation, we found that cold air (−1 K) sitting above the edge of a deep warm core (+1.5 K) can increase the near-surface pressure difference between the inner and outer regions of TCs by 3–4 mbar, potentially increasing the maximum winds in a typical hurricane by 4–10 kt (using an empirical relationship from *Courtney and Knaff* [2009]).

At maximum intensity, cold air masses extend as far as 1000 km away from the storm center. This may be significant for meridional heat and moisture transport: while the warm core transports heat and water vapor poleward in the troposphere, there may be a significant poleward transport of cold, dry air in the UTLS originating in the tropics.

Acknowledgments

The authors thank Brian Bevirt, Editor at the National Center for Atmospheric Research (NCAR), Wayne Schubert, Christopher Slocum, and two anonymous reviewers, whose comments greatly helped the revision of the first manuscript. This work is supported through Colorado State University's Programs of Research and Scholarly Excellence. The COSMIC Data Analysis and Archive Center (CDAAC) is supported by the National Science Foundation under NSF award AGS-1033112 and AGS-1522830. GPS-RO data are available at http://cdaac-www.cosmic.ucar.edu. AMSU-A and IR data used in this study are available upon request to John Knaff (john.knaff@noaa.gov). The views, opinions, and findings contained in this report are those of the authors and should not be construed as an official National Oceanic and Atmospheric Administration or U.S. Government position, policy, or decision.

References

Arakawa, H. (1951), Analysis of the tropopause and the stratospheric field of temperature of a mature typhoon, *Pap. Meteorol. Geophys.*, *2*(1), 1–5.

Biondi, R., W. Randel, S.-P. Ho, T. Neubert, and S. Syndergaard (2012), Thermal structure of intense convective clouds derived from GPS radio occultations, *Atmos. Chem. Phys.*, *12*(12), 5309–5318.

Biondi, R., S.-P. Ho, W. Randel, S. Syndergaard, and T. Neubert (2013), Tropical cyclone cloud-top height and vertical temperature structure detection using GPS radio occultation measurements, *J. Geophys. Res. Atmos.*, *118*, 5247–5259, doi:10.1002/jgrd.50448.

Buontempo, C., H. Flentje, and C. Kiemle (2006), In the eye of a tropical cyclone, *Weather*, *61*(2), 47–50.

Courtney, J., and J. A. Knaff (2009), Adapting the Knaff and Zehr wind-pressure relationship for operational use in tropical cyclone warning centres, *Aust. Meteorol. Oceanogr. J.*, *58*(3), 167.

Davis, N., and T. Birner (2016), Climate model biases in the width of the tropical belt, *J. Clim.*, *29*(5), 1935–1954.

Demuth, J. L., M. DeMaria, J. A. Knaff, and T. H. Vonder Haar (2004), Evaluation of Advanced Microwave Sounding Unit tropical-cyclone intensity and size estimation algorithms, *J. Appl. Meteorol.*, *43*(2), 282–296.

Demuth, J. L., M. DeMaria, and J. A. Knaff (2006), Improvement of Advanced Microwave Sounding Unit tropical cyclone intensity and size estimation algorithms, *J. Appl. Meteorol. Climatol.*, *45*(11), 1573–1581.

Emanuel, K., and R. Rotunno (2011), Self-stratification of tropical cyclone outflow. Part I: Implications for storm structure, *J. Atmos. Sci.*, *68*(10), 2236–2249.

Emanuel, K. A. (1991), The theory of hurricanes, *Annu. Rev. Fluid Mech.*, *23*(1), 179–196.

Frank, W. M. (1977), The structure and energetics of the tropical cyclone: I. Storm structure, *Mon. Weather Rev.*, *105*(9), 1119–1135.

Gettelman, A., P. Hoor, L. Pan, W. Randel, M. Hegglin, and T. Birner (2011), The extratropical upper troposphere and lower stratosphere, *Rev. Geophys.*, *49*, RG3003, doi:10.1029/2011RG000355.

Goldberg, M. D., D. S. Crosby, and L. Zhou (2001), The limb adjustment of AMSU-A observations: Methodology and validation, *J. Appl. Meteorol.*, *40*(1), 70–83.

Heymsfield, G. M., J. B. Halverson, J. Simpson, L. Tian, and T. P. Bui (2001), ER-2 Doppler radar investigations of the eyewall of Hurricane Bonnie during the Convection and Moisture Experiment-3, *J. Appl. Meteorol.*, *40*(8), 1310–1330.

Holloway, C. E., and J. D. Neelin (2007), The convective cold top and quasi equilibrium, *J. Atmos. Sci.*, *64*(5), 1467–1487.

Johnson, R. H., and D. C. Kriete (1982), Thermodynamic and circulation characteristics, of winter monsoon tropical mesoscale convection, *Mon. Weather Rev.*, *110*(12), 1898–1911.

Knaff, J. A., R. M. Zehr, M. D. Goldberg, and S. Q. Kidder (2000), An example of temperature structure differences in two cyclone systems derived from the Advanced Microwave Sounder Unit, *Weather Forecasting*, *15*(4), 476–483.

Knaff, J. A., S. P. Longmore, and D. A. Molenar (2014), An objective satellite-based tropical cyclone size climatology, *J. Clim.*, *27*(1), 455–476.

Koteswaram, P. (1967), On the structure of hurricanes in the upper troposphere and lower stratosphere, *Mon. Weather Rev.*, *95*(8), 541–564.

Kuo, Y.-H., T.-K. Wee, S. Sokolovskiy, C. Rocken, W. Schreiner, D. Hunt, and R. Anthes (2004), Inversion and error estimation of GPS radio occultation data, *J. Meteorol. Soc. Jpn.*, *82*(1B), 507–531.

Kursinski, E., et al. (1996), Initial results of radio occultation observations of Earth's atmosphere using the Global Positioning System, *Science*, *271*(5252), 1107–1110.

Kursinski, E. R., G. A. Hajj, S. Leroy, and B. Herman (2001), The GPS radio occultation technique, *Terr. Atmos. Oceanic Sci.*, *1*, 53–114.

Molinari, J., P. Duran, and D. Vollaro (2014), Low Richardson number in the tropical cyclone outflow layer, *J. Atmos. Sci.*, *71*(9), 3164–3179.

Möller, J. D., and M. T. Montgomery (2000), Tropical cyclone evolution via potential vorticity anomalies in a three-dimensional balance model, *J. Atmos. Sci.*, *57*(20), 3366–3387.

Paulik, L. C., and T. Birner (2012), Quantifying the deep convective temperature signal within the tropical tropopause layer (TTL), *Atmos. Chem. Phys.*, *12*(24), 12,183–12,195.

Pendergrass, A. G., and H. E. Willoughby (2009), Diabatically induced secondary flows in tropical cyclones. Part I: Quasi-steady forcing, *Mon. Weather Rev.*, *137*(3), 805–821.

Reasor, P. D., M. T. Montgomery, and L. D. Grasso (2004), A new look at the problem of tropical cyclones in vertical shear flow: Vortex resiliency, *J. Atmos. Sci.*, *61*(1), 3–22.

Rogers, R., P. Reasor, and S. Lorsolo (2013), Airborne Doppler observations of the inner-core structural differences between intensifying and steady-state tropical cyclones, *Mon. Weather Rev.*, *141*(9), 2970–2991.

Sampson, C. R., and A. J. Schrader (2000), The automated tropical cyclone forecasting system (version 3.2), *Bull. Am. Meteorol. Soc.*, *81*(6), 1231–1240.

Schubert, W. H., and B. D. McNoldy (2010), Application of the concepts of Rossby length and Rossby depth to tropical cyclone dynamics, *J. Adv. Model. Earth Syst.*, *2*, 7.

Seidel, D. J., R. Ross, J. K. Angell, and G. C. Reid (2001), Climatological characteristics of the tropical tropopause as revealed by radiosondes, *J. Geophys. Res.*, *106*(D8), 7857–7878.

Son, S.-W., N. F. Tandon, and L. M. Polvani (2011), The fine-scale structure of the global tropopause derived from COSMIC GPS radio occultation measurements, *J. Geophys. Res.*, *116*, D20113, doi:10.1029/2011JD016030.

Steranka, J., E. B. Rodgers, and R. C. Gentry (1986), The relationship between satellite measured convective bursts and tropical cyclone intensification, *Mon. Weather Rev.*, *114*(8), 1539–1546.

Stern, D. P., and D. S. Nolan (2009), Reexamining the vertical structure of tangential winds in tropical cyclones: Observations and theory, *J. Atmos. Sci.*, *66*(12), 3579–3600.

Weatherford, C. L., and W. M. Gray (1988), Typhoon structure as revealed by aircraft reconnaissance. Part II: Structural variability, *Mon. Weather Rev.*, *116*(5), 1044–1056.

Willoughby, H. (1998), Tropical cyclone eye thermodynamics, *Mon. Weather Rev.*, *126*(12), 3053–3067.